ORIGINAL PAPER

Effect of simultaneous N$_2$ collisions on atomic oxygen-induced polyimide erosion in sub-low Earth orbit: comparison of laboratory and SLATS data

Kumiko Yokota^1 · Masahito Tagawa^1 · Yusuke Fujimoto^1 · Wataru Ide^1 · Yugo Kimoto^2 · Yuta Tsuchiya^2 · Aki Goto^2 · Kazuki Yukumatsu^2 · Eiji Miyazaki^2 · Shunsuke Imamura^2

Abstract

The role of N$_2$ in the upper atmosphere on the atomic oxygen (AO)-induced erosion of polyimide in low Earth orbit (LEO) and sub-LEO is investigated through ground-based experiments and flight data. The experiment is performed by adding an Ar beam at the same collision energy as an undecomposed O$_2$ component in the AO beam formed by laser detonation to simulate the physical effect of simultaneous N$_2$ collision in sub-LEO. The Ar beam is added by the dual-pulsed supersonic valve-equipped laser-detonation system developed at Kobe University. The experimental results indicate that the erosion of polyimide in the laser-detonation system is promoted by the presence of O$_2$ and Ar in the beam, corresponding to N$_2$ in the sub-LEO. On-ground experimental results are compared with in-orbit AO measurements. Previous space shuttle, international space station-based exposure experiments, as well as the world's first real-time sub-LEO material erosion data aboard a super low altitude test satellite (SLATS) orbiting at an altitude of 216.8 km are presented. The SLATS data suggests the presence of an acceleration effect by N$_2$ collision on AO-induced polyimide erosion, as predicted by ground-based experiments.

Keywords Low Earth orbit · Material degradation · SLATS · Atomic oxygen · Nitrogen

1 Introduction

It has been widely recognized that many polymeric materials used in spacecraft and systems are eroded by hyperthermal (4.5 eV) collisions of atomic oxygen (AO) in low Earth orbit (LEO). Many flight and ground-based experiments have been performed to investigate the survivability of materials in harsh AO environments in LEO. Many ground-based studies used laser-detonation AO beam sources to simulate energetic AO collisions in LEO. However, it has been reported that erosion yields of materials relative to polyimide (Kapton-H) measured in a ground-based facility are often not consistent with those measured by flight experiments in LEO [1].

This phenomenon is evident in fluoropolymers. The origin of the inconsistency has been investigated extensively. The effect of ultraviolet (UV) emission from laser-induced oxygen plasma has been considered as the origin of the accelerated erosion of fluoropolymers in ground-based facilities [2]. However, the acceleration of AO-induced erosion of polyimide via simultaneous UV irradiations, i.e., the synergistic effect, has not been observed in fluoropolymers, but in polyimide [3]. The acceleration of the AO-induced erosion of a fluoropolymer is currently considered assumed to be caused by the energetic collision of undecomposed O$_2$ in an AO beam formed by a laser detonation source [4].

Meanwhile, the acceleration of AO-induced polyimide observed via UV irradiation can be explained by the two-stage reaction of hydrocarbon polymers with AO; the first stage is the oxidation process and the second is the desorption process [5]. The acceleration effect of the AO-induced erosion of polyimide may be observed in environments where the desorption process, which is a rate-limiting step, is promoted by any type of stimulus, such as UV or particle

✉ Kumiko Yokota
   yokota@mech.kobe-u.ac.jp

✉ Masahito Tagawa
   tagawa@mech.kobe-u.ac.jp

1   Kobe University, Rokko-dai 1-1, Nada, Kobe 657-8501, Japan

2   Japan Aerospace Exploration Agency, Sengen 2-1-1, Tsukuba 305-8505, Japan

bombardment. In fact, the accelerated erosion of polyimide by collision-induced desorption (CID) process has been reported by Minton et al. [6, 7]. They observed a 30% increase in CO/CO_2 signals from an Ar bombarded surface.

Based on the abovementioned studies, material erosion at a very low altitude of 200 km or less, which is known as sub-LEO, should differ from those in LEO at 400 km. This is because the N_2 fraction exceeds 50% in sub-LEO compared with a few percent in LEO. Because of its large mass, the collision energy of N_2 exceeds 9 eV, which is effective for accelerating the desorption of reaction products from oxidized hydrocarbon surfaces. The same phenomenon is expected from undecomposed O_2 in the laser detonation AO exposure testing on the ground. However, the effects of high-energy N_2 or O_2 collisions on material erosion tests have not been considered.

The acceleration of erosion on polyimide is important because polyimide is the reference material to evaluate the AO-induced erosion yield of other materials in all material survivability tests both in orbit and on the ground. Moreover, even if the erosion of polyimide had accelerated, it might not have been recognized since erosion of polyimide had always been regarded as 3.0E-24 cm^3/atom in all test conditions.

In this study, we evaluated the effect of high-energy collision of chemically inert atoms/molecules during AO exposure on polyimide. A dual-beam laser-detonation beam facility was specially designed and developed for this purpose. The ground-based results were compared with flight experiments flown by a space shuttle (STS) and the International space station (ISS). Preliminary data of the world's first real-time polyimide erosion measurement in a sub-LEO environment aboard a super-low altitude test satellite (SLATS) are reported as well.

2 Ground-based experiments

A ground-based experiment was performed by adding Ar beam pulses at the same collision energy as the O_2 component in the AO beam. Ar was used to avoid the decomposition of N_2 in the laser-induced plasma, which would decrease of the collision energy. The chemical nature of N_2 was disregarded, and only the physical effect of N_2 collision in orbit was simulated. An Ar beam was added using a dual-pulsed supersonic valve (PSV) laser detonation system. Figure 1 shows the dual-PSV system especially developed in this study. The entire facility was composed of three vacuum chambers: source, reaction, and time-of-flight (TOF) chambers. These chambers were evacuated by turbomolecular pumps. AO production and normal exposure tests were performed in the source chamber, experiments requiring high-vacuum were performed in the reaction chamber, and the energy of atoms was analyzed in the TOF chamber.

The dual-PSV was equipped to the source chamber (Fig. 1). Two piezoelectric transducers (PZTs) were equipped installed in the dual-PSV system. Low-voltage PZTs with a displacement enlargement mechanism were installed [8, 9]. The operating voltage of the PZT was 150 V which was lower than that of a disk-type transducer (e.g., 1 kV). The low operation voltage prevented unexpected discharges from the PZT. These mechanisms were installed in a stainless steel body. The target gas was ejected through a 1 mm channel, and sealing was enabled using a Viton O-ring. The poppet clearance was adjustable using a micrometer. The poppet system with a Viton O-ring and Au reflector was specially designed for laser-detonation applications, as it was required by the focusing 7 J laser pulse near the O-ring. Two PSVs were attached to the nozzle throat at 45° with respect to the beam axis. The distance of the Viton O-ring to the nozzle throat was minimized to 5 mm to ensure the rapid introduction of gas pulses into the nozzle. Because both Ar and AO+O_2 beams were formed in the same nozzle, the incident angles of both beams were identical, i.e., they generated normal incidence.

To avoid the interference of pulse timing, two system clocks (TTL signal) with a phase difference of 180° were used for each PSV. One of the TTL signals was decimated for tuning the flux ratio of the gases. The TTL signals were converted to the designated shape of the PSV driving signals using function generators, and the driving signals were amplified using PSV drivers. The laser firing timings for the two gases were individually adjusted using digital delay generators. Both delayed signals were connected to a CO_2 laser. The maximum repetition rate of the dual-PSV exceeded over 50 Hz, however, the system repetition rate was restricted by that of the CO_2 laser (5 Hz).

The material targeted was pyromellitic dianhydride oxydianiline (PMDA-ODA) polyimide varnish which has the same repeating unit as Kapton-H (Toray-DuPont, Semicofine SP-341). The polyimide film was spin-coated on a quartz crystal microbalance (QCM) sensor crystal at 800 rpm for 1 min, and curing treatments were performed at 150 °C for 1 h and 300 °C for 1 h in N_2. The curing process was performed to form a polyimide structure with a thickness of approximately 1 μm. The erosion of polyimide was calculated from the frequency shift of the polyimide-coated QCMs located 52 cm away from the nozzle throat at room temperature with normal incidence.

3 Results of ground-based experiment

Figure 2 shows the TOF distributions of the AO, undecomposed O_2, and Ar components in the beam. The average translational energies of AO, O_2, and Ar were 2.9, 4.0 and 4.0 eV, respectively. The average translational energy of
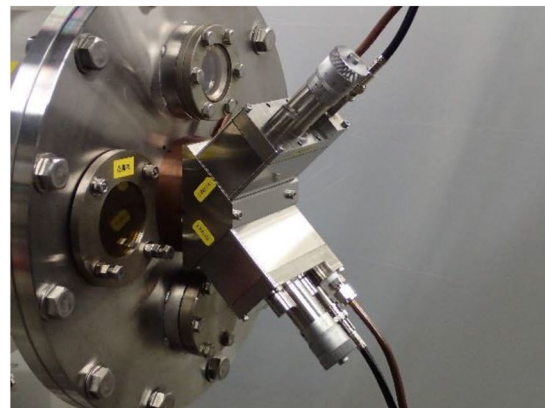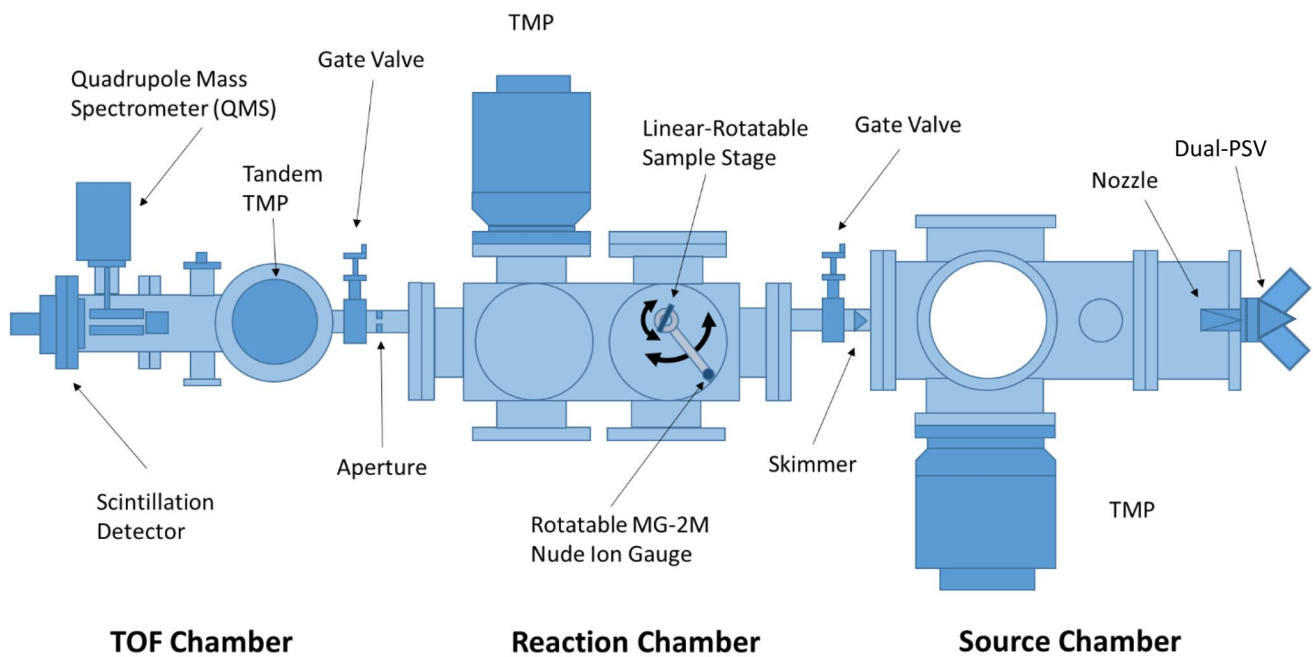
Fig. 1 Schematics of the laser detonation AO beam source at Kobe University. Photograph inserted is the dual-PSV system used in this experiment [8]

Ar was set to a relatively low value compared with the N_2 energy in a real space environment. It was used to simulate the physical effect of O_2 in the beam. The flux of AO was measured from the mass loss of polyimide-coated QCM, whereas Ar and O_2 were calculated from the area of flux-weighted TOF distributions with known relative ionization cross-sections of AO, O_2, and Ar [10]. Relative errors due to noise and integration of the flux-weighted TOF distribution area were evaluated by changing the smoothing level and the upper limits of the integration. It was determined that the relative error in smoothing and area integration was less than 2 and 5%, respectively. Therefore, the total uncertainty of the

fraction of high-energy molecules should be less than 10%. Meanwhile, the mass loss calculated from the frequency shift of the QCM was measured via linear regression. It was observed that the mass loss of the polyimide was stable during the exposure, as shown in Fig. 2d.

Figure 3 shows the relationship between the fraction of high-energy molecules (O_2 + Ar) and the relative erosion rate of polyimide measured from the frequency shift of the polyimide-coated QCM. The data point of 0.257 in the abscissa is that of the AO beam without Ar pulses. The ordinate was normalized by the erosion rate of AO + O_2 beam pulses without adding Ar pulses. It is clear that the
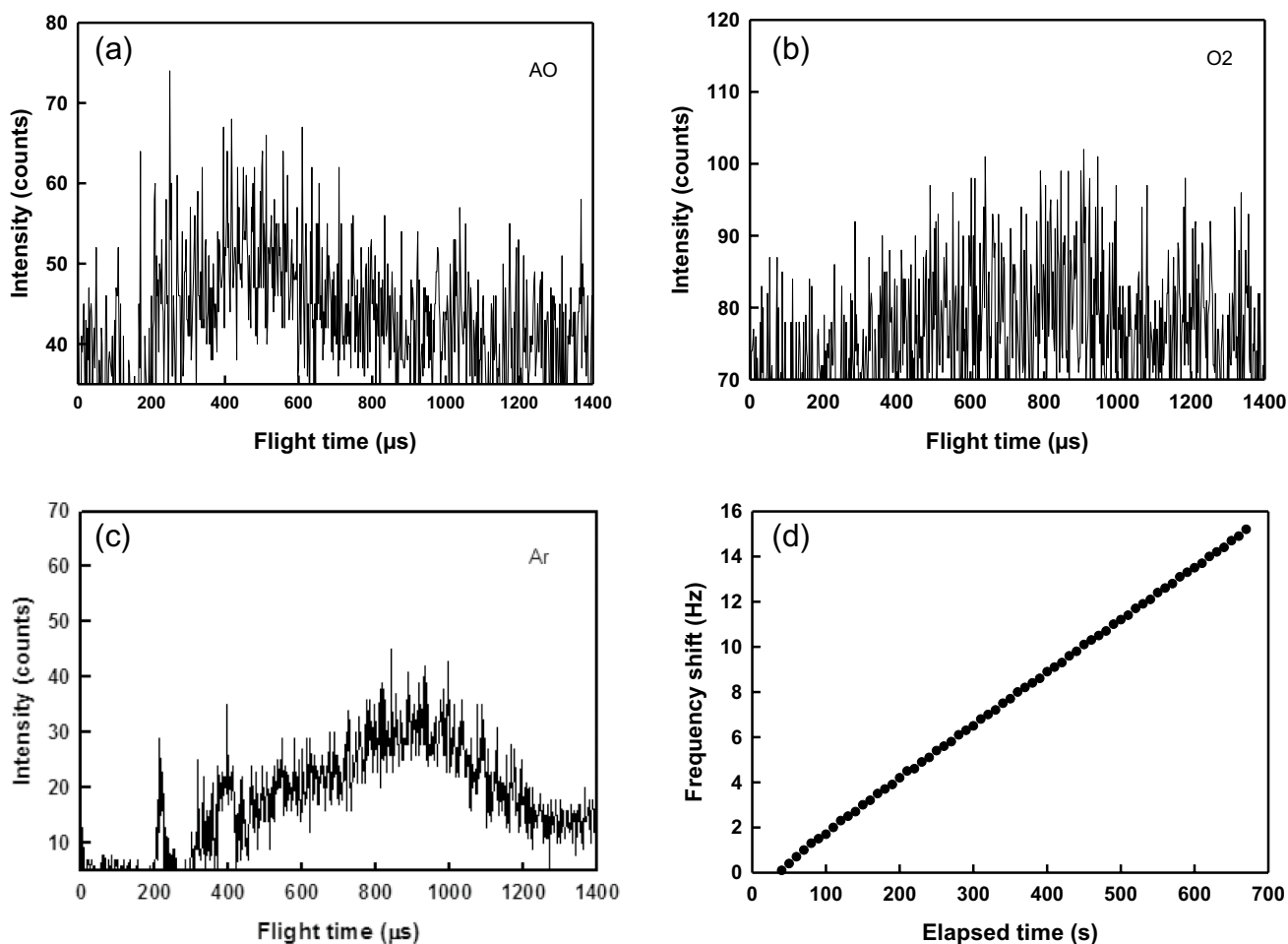
Fig. 2 Time-of-flight spectra (TOF) and frequency shift of polyimide-coated QCM during the exposure. **a**: TOF of AO, **b**: TOF of O_2, **c**: TOF of Ar, **d**: Frequency shift of polyimide-coated QCM. Average translational energies are set to 2.9 eV for AO, 4.0 eV for O_2 and 4.0 eV for Ar, respectively. Stable erosion of the mass-loss of polyimide was observed in (**d**)
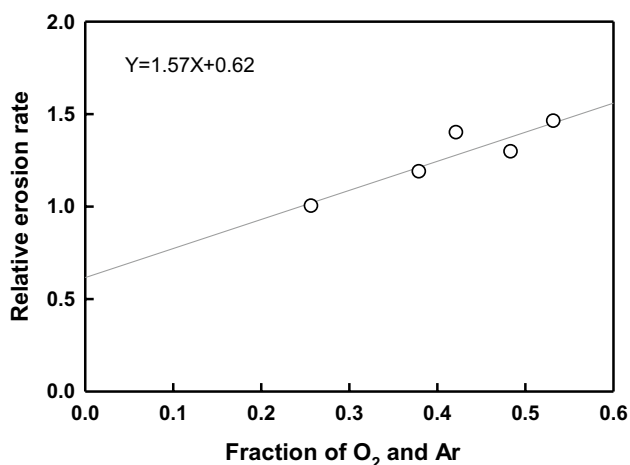

Fig. 3 Relationship between the fraction of Ar + O_2 in the beam and the relative erosion rate of polyimide. The longitude is normalized by the erosion rate with AO beam including undecomposed O_2 component (Ar beam pulse is not used)

erosion rate of polyimide increased was Ar pulses were added. The increase in the relative erosion rate was almost linear with respect to the fraction of high-energy particles (O_2 + Ar) in the range of 0.25–0.55. This is expected as CID is the rate-limiting step of the mass loss [7]. By extrapolating the linear fitting results, the net erosion rate of polyimide by the AO component (without the effect of O_2 collision) was 62% of the conventional AO beam used for the ground-based experiments. In other words, polyimide erosion in the laser detonation AO beam source accelerated by 1.6 times owing the presence of the O_2 component in the beam. As the AO beam formed by the laser-detonation system typically includes 30–50% O_2 depending on the condition, the mass loss of the Kapton witness samples exposed to the AO beam in the ground-based experiments is improved; i.e., the fluence of AO was over-estimated by 1.5–2 times when measured using the Kapton witness sample.

4 Kapton erosion yield measurements in previous flight missions

Kapton-H has been used for measuring the fluence of AO exposures for many years. The standard erosion yield (Ey) of 3.0E-24 cm^3/atom has been recommended for measuring the flux of AO in ASTM standard E-2089 [11]. The value of 3.0E-24 cm^3/atom was obtained through measurement in early STS flights. The STS-8 mission at an altitude of 225 km provided some of the first meticulously characterized Ey values, with Kapton Ey values of 3.0E-24 cm^3/atom including Banks [12] and Visentine [13]. This value has been applied for all space missions and ground-based experiments as a reference. However, the N$_2$ fraction at 225 km reached as high as 33% according to an atmospheric model analysis of the Naval Research Laboratory Mass Spectrometer Incoherent Scatter Extended model (NRLMSISE-00). The acceleration effect of the AO-induced erosion of polyimide due to simultaneous N$_2$ collisions mentioned in the previous section was not considered in this established value. If the experimental results shown in the previous section are correct, then the standard Ey of 3.0E-24 cm^3/atom for polyimide may be accelerated by the simultaneous N$_2$ collisions at an altitude of 225 km, and the acceleration effect would depend on the altitude of the N$_2$ fraction.

We have searched reports of past flight experiments aboard STSs and the ISS to compare the difference in predicted and measured AO fluences from polyimide erosion. Only a few related reports have been published, however, some examples are listed in Table 1. It was obvious that the AO fluences measured by Kapton-H and calculated using the MSIS-86 atmospheric model [14] agreed well for EOIM-3 on STS-46 [15]; however, NRLMSISE-00 predictions of AO fluence were overestimated in the JEM/MPAC&SEED [16] and MEDET [17] on the ISS. It is noteworthy that the NRLMSISE-00 model is the latest version of the MSIS-86 model [18]. The abovementioned phenomenon may be explained by the lack of N$_2$ effect on ISS-based experiments. The acceleration of erosion due to N$_2$ collision was apparent based on Table 1, even though the AO fluences for ISS missions cannot be accurately predicted easily because of the complex nature of predicting the shielding effect when modeling the AO fluence of the long-term ISS-mounted sample [19].

5 AOFS mission aboard SLATS

Real-time erosion measurement of polyimide in a sub-LEO environment was first performed by the atomic oxygen fluence sensor (AOFS) mission aboard SLATS launched on December 23, 2017. The AOFS mission was composed of five polyimide-coated QCMs. Details regarding the SLATS and AOFS mission have been reported elsewhere [20, 21]. We analyzed the telemetry data of the frequency shift of the QCM sensors (AOFS-H5 and H7) attached to the + z surface (Earth-facing side) of the SLATS (facing the + x direction) and the + x surface (front surface), as shown in Fig. 4. AOFS-H5 and H7 were equipped with shutter mechanisms for the long-life operation of polyimide-coated QCMs in a dense AO environment. The frequency data of H5 polyimide-coated QCMs (U-varnish A, Ube) in the period from July 23, 2019 to August 26, 2019, at an altitude of 216.8 km, and that of H7 from June 2, 2019 to July 23, 2019, at an altitude of 250–216.8 km were analyzed. It is noteworthy that the normal solar activity periods during the shutter opening were selected for the analysis.

The frequency shift of the QCM, which is proportional to the mass loss of polyimide every 3 min, was analyzed using Sauerbrey's equation below [22].

$$\Delta f = -\frac{2N f_0^2 \Delta m}{A_E \sqrt{\mu \rho}}$$

where: Δf: frequency shift of the QCM, N the harmonic overtone, f_0 the resonant frequency, Δm the mass loss of polyimide, A_E the electrode area, μ the shear modulus of the quartz, and ρ the density of the quartz. Meanwhile, the AO fluence $\left(F_{AO}\right)$ was calculated by multiplying the AO density predicted by NRLMSISE-00 atmospheric model and the traveling distance of the satellite from GPS data. The erosion yield (Ey) of polyimide was calculated using the equation below.

$$Ey = \frac{\Delta m}{F_{AO}\, \rho_{PI}\, A}$$

where: ρ_{PI} the density of polyimide, and A the area of polyimide.

Table 1 Comparison of AO fluences predicted by MSIS atmospheric model and measured from Kapton erosion in various flight missions

Mission	Year	Platform	Atomic oxygen fluences (atoms/cm^2)		
			Kapton-equiv.	MSIS prediction	Ratio
EOIM-3	1986	STS-46	2.40E+20	2.10E+20	1.14
MEDET	2008	ISS	1.70E+21	2.30E+21	0.71
JM/MPAC&SEED	2010	ISS	5.90E+20	1.40E+21	0.42

Fig. 4 Artistic image of superlow altitude test satellite (SLATS) and its photograph before launch. AOFS-H5 and H7 QCM sensor locations are indicated by the red circles
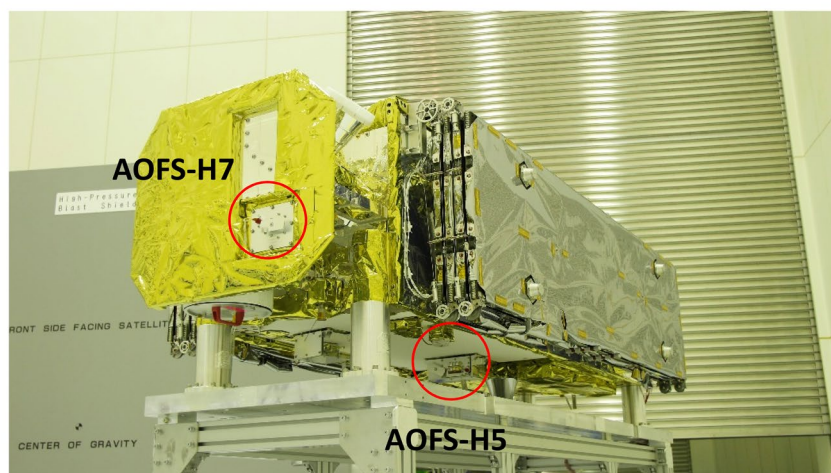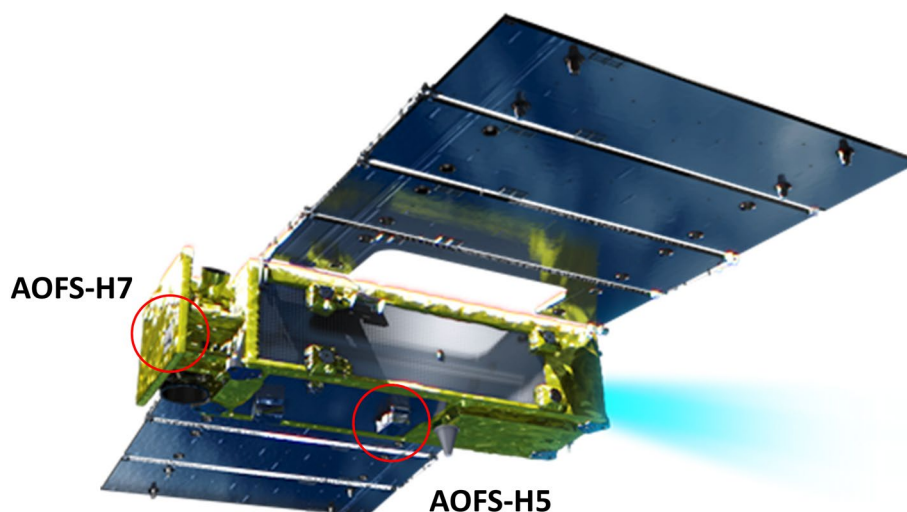

Figure 5 shows the AO and N_2 densities in the SLATS orbit predicted by the NRLMSISE-00 atmospheric model as a function of latitude. The NRLMSISE-00 calculation was performed based on the actual SLATS flight data (date, time, longitude, latitude, altitude and solar activity) every 10 s. The density of AO and N_2 calculated subsequently were averaged for 3 min. which is the same period of the QCM measurement and plotted (as shown in Fig. 5). The negative and positive latitude values in Fig. 5 represent the southern and northern hemispheres, respectively. It is clear that the AO density predicted by the NRLMSISE-00 model was not constant in the orbit. This was primarly because the altitude of the SLATS changed based on the latitude. Hence, the distribution of the AO density was symmetric across the equator. Meanwhile, the N_2 density decreased in the southern hemisphere with the latitude but increased in the northern hemisphere. This was likely due
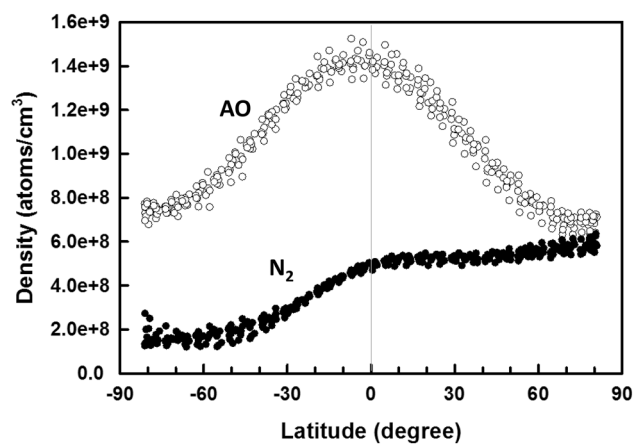

Fig. 5 Example of AO and N_2 density distributions in SLATS orbit as a function of latitude on August 12–26, 2019 when the shutter opens. Asymmetric distribution of N_2 is due to the ascending current N_2 heated by the Sun in the northern hemisphere

to the ascending current of N$_2$ heated by the Sun during the summer in the northern hemisphere. This phenomenon has been observed in the upper atmosphere at the local time of 15–18 h during the summer [23]. The total mass density of the atmosphere predicted by NRLMSISE-00 was compared with those predicted by the Jacchia-Bowman model (JB2008) [24] and the drag temperature model (DTM2013) [25]. A similar distribution was predicted by the other two atmospheric models, suggesting that the unusual dense N$_2$ concentration was qualitatively correct. The SLATS orbited this unusual condition owing to its operation requirement: dawn-dust orbit (local time of 16 h) from June to August 2019. According to the NRLMSISE-00 prediction, the N$_2$ fraction in the SLATS orbit changed from 15 to 50% in each cycle of orbiting.

Figure 6 shows the relative Ey calculated by the mass loss of polyimide on the QCM as a function of N$_2$ fraction in the atmosphere predicted by NRLMSISE-00. The black triangles shown in Fig. 6 were values normalized by 3.0E-24 cm^3/atom at 33% N$_2$ fraction (STS-8 condition). The grey circles represent the AOFS-H5 data, whereas the

white squares represent data from AOFS-H7. The ground experimental data and AOFS-H7 data showed an increase in Ey as the fraction of high-energy particles increased. By contrast, the AOFS-H5 data showed a breakpoint at the high-energy particle of 25%, then decreased as the fraction of the high-energy particles increased. As the AOFS-H5 was located on the bottom surface of the SLATS, the shielding effect of the fuselage of the SLATS may affect the AOFS-H5 data, even though only the data points with positive pitch angles were plotted in Fig. 6 (nose-up attitude). The shielding effect of AOFS-H5 must be analyzed in detail in future analyses. Meanwhile, the AOFS-H7 data did not affect the shielding effect; therefore, we compared the AOFS-H7 data with results from the ground-based experiments. No breaking point was observed in the AOFS-H7 data as shown in Fig. 6 i.e., Ey linearly increased with N$_2$ fraction. However, the absolute value of Ey in the ground experimental data normalized by the STS-8 and AOFS-H7 data were not coincident as shown in Fig. 6. This was due to many uncertain factors, such as the inaccuracy of NRLMSISE-00 atmospheric model predictions. Therefore, we focused only on the slope of these data plots here. The two lines in Fig. 6 show the linear regressions performed on the ground experiment results and AOFS-H7 data. The linear regression results in Fig. 6 were normalized by Ey without high-energy particles and are indicated in Table 2. The relative changes in Ey on these lines were almost identical within an error of 4%. That the AOFS-H7 data showed a slightly more prominent effect than the ground-based experiment was attributable to the higher collision energy of N$_2$ in sub-LEO than that of Ar in the ground experiment. However, the effect of the difference in collision energy, i. e., between 4.0 eV of Ar in the ground experiment and 9 eV in N$_2$ in the sub-LEO was relatively small. The reason is yet to be elucidated, however, the Ar energy (4.0 eV) would be in sufficient to detect the effect of collision energy as the threshold of the CID is reported to be 8 eV [6]. Table 2 suggests that the Kapton erosion at 200 km in altitude, where the N$_2$ fraction reached approximately 50%, is 1.8 times greater than that in the ISS orbit where the N$_2$ fraction is less than a few percent. In other words, the Kapton-equivalent AO fluence in sub-LEO overestimates the AO fluence. Based on Fig. 6 and Table 2, it is clear that the effect of high-energy particles on the AO-induced erosion predicted via the ground-based experiment [4] was accurate, as confirmed by the flight experiment aboard SLATS.
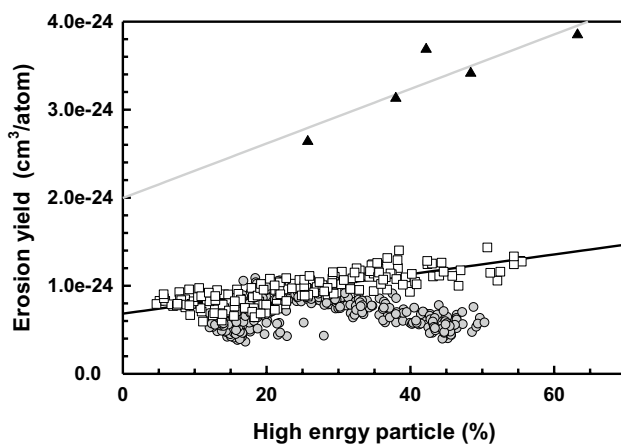

Fig. 6 Erosion yield (Ey) of polyimide obtained in the laboratory, AOFS-H5 and H7sensors as a function of high energy particle fraction. Note that Ey of laboratory data (black triangles) are normalized to be 3.0E-24 cm^3/atom at 33% N$_2$ based on the STS-8 results. Grey circles and white squares show AOFS-H5 and H7 data based on the mass-loss calculated from Sauerbrey's equation and AO density predicted by the NRLMSISE-00 atmospheric model, respectively. Linear regression results are shown in the solid lines; $Y = 3.01E-26X + 2.00E-24$ (experiments) and $Y = 1.12E-26X + 6.83E-25$ (AOFS-H7)

Table 2 Relative increase in erosion yields (Ey) by high-energy particles estimated by the laboratory experiment and AOFS-H7 data. Ey are normalized by the 0% high-energy particle condition

High-energy particle (%)	0	10	20	30	40	50
Ey predicted by Laboratory data	1.00	1.15	1.30	1.45	1.60	1.75
Ey measured by AOFS-H7	1.00	1.16	1.33	1.49	1.66	1.82

6 Conclusions

We analyzed the effect of hyperthermal collisions of N_2 on AO-induced polyimide erosion in a sub-LEO space environment. Collisions of N_2 were simulated by an Ar beam formed by a dual-PSV system in a ground-based experiment. Laboratory results clearly indicated that the erosion rate of polyimide increased linearly with the fraction of high-energy particles (N_2, O_2, or Ar). Because the established erosion yield of polyimide, 3.0E-24 cm^3/atom, was measured at 240 km in altitude (N_2 fraction of 33%) by the STS-8, the polyimide erosion on the ISS at an altitude of 450 km would be smaller than that at 240 km. This tendency was confirmed by flight experiments conducted on STS and ISS, even though the accurate estimation of AO fluence was difficult. Meanwhile, SLATS/AOFS data, which is the world's first material erosion data in sub-LEO, were analyzed from the viewpoint of the acceleration effect of N_2 on AO-induced polyimide erosion. AOFS-H7 data, which do not require the consideration of the shielding effect of the SLATS fuselage, agreed well with the ground-based experiment. A series of ground and flight experimental results suggested that the erosion of polyimide in sub-LEO was greater than that predicted by AO fluence with a constant Ey of 3.0E-24 cm^3/atom.

References

1. Weihs B., van Eesbeek, M.: Secondary VUV erosion effect on polymers in the ATOX atomic oxygen exposure facility. In: Proceedings of the 6th International Symposium in Materials in a Space Environment, ESA SP-368, pp.277–283. Noordwijk, The Netherlands (1994)

2. van Eesbeek, M., Levadau, F., Skurat, V.E., Dorofeev, Y.I., Vasilets, V.N., Babashev, E.A.: Degradation of Teflon FEP due to VUV and atomic oxygen exposure. In: Proceedings of the 6th International Symposium in Materials in a Space Environment, ESA SP-368, pp. 165–173. Noordwijk, The Netherlands (1994)

3. Tagawa, M., Yokota, K., Kishida, K., Okamoto, A., Ishizawa, J., Minton, T.K.: Effect of ultraviolet emission from the oxygen plasma on the accelerated erosion phenomenon of fluorinated polymer in the atomic oxygen ground tests. High Perform. Polym. **22**(2), 213–224 (2010)

4. Tagawa,, M., Ide, K., Yamasaki, Y., Watanabe, D., Hatsuda, A., Yokota, K.: Effect of high-energy inert gas collisions on the atomic oxygen-induced polymer erosion. In: Proceedings of 13th International Symposium in Materials in a Space Environment (2015) on CD-ROM (2015)

5. Kenoshita, H., Tagawa, M., Yokota, K., Ohnae, N.: Nonlinear phenomenon in the mass-loss of polyimide film under hyperthermal atomic oxygen beam exposure. High Perform. Polym. **13**, 225–234 (2001)

6. Minton, T.K., Garton, D.J.: Dynamics of atomic-oxygen-induced polymer degradation in low earth orbit. In: Dressler, R.A. (ed.) Advanced series in physical chemistry. Chemical dynamics in extreme environments, vol. 11, pp. 420–489. World Scientific, Singapore (2001)

7. Minton, T.K., Zhang, J., Garton, D.J., Seal, J.W.: Collision-assisted erosion of hydrocarbon polymers in atomic-oxygen environment. High Perform. Polym. **12**, 27 (2000)

8. Yokota, K., Kita, K., Okura, R., Shimizu, T., Chee, S.K., Iwata, M., Tagawa, M.: One-nozzle two-beam laser-detonation system. In: 14th International Symposium on Materials in the Space Environment/12th International Conference on protection of Materials and Structures in a Space Environment. Biarritz, France (2018)

9. Yokota, K., Tagawa, M.M., Kleiman, J.I.: Atomic oxygen exposure test capabilities at Kobe University: its performance and limitations. In: Proceedings of Advanced Space Environmental Conference, Universal City USA, (2019)

10. Yokota, K., Yasuda, S., Mizutani, A., Tagawa, M.: Relative electron impact ionization probabilities of O, O_2 and Ar components in the laser-detonation hyperthermal beams. Jpn. J. Appl. Phys. **52**, 038002 (2013)

11. Standard practices for ground laboratory atomic oxygen interaction evaluation of materials for space applications, ASTM E2089–00 (2006)

12. Banks, B.A., Mirtich, M.J., Rutledge, S.K., Swec, D.M.: Sputtered coatings for protection of spacecraft polymers, Thin Solid Films, 127 (1985), 107–114. Also Visentine, J.T., Leger, L.J., Kuminecz, J.F., Spiker, I. K.: STS-8 atomic oxygen effects experiment, AIAA-85-0415 (1985

13. Visentine, J.T., Leger, L.J., Kuminecz, J.F., Spiker, I. K.: STS-8 atomic oxygen effects experiment, AIAA-85-0415 (1985)

14. Hedin, A.E.: MSIS-86 thermospheric model. J. Geophys Research **92**(A5), 4649–4662 (1987)

15. Brinza, D.E., Chung, S.Y., Minton, T.K., Liang, R.H.: Final report on the NASA/JPL evaluation of oxygen interactions with materials 3 (EOIM-3), JPL Publication 94–31 (1994)

16. Kimoto, Y., Ishizawa, J., Shimamura, H.: Passive space environment effect measurement on JEM/MPAC&SEED. In: Kleiman, J.I., Tagawa, M., Kimoto, Y. (eds.) Protection of materials and structures from the space environment, p. 73. Springer, Heidelberg (2013)

17. Rejsek-Riba, V., Soonckindt, S., Duzellier, S., Remaury, S., Durin, C., Desmarres, J.M., Tighe, A., van Eesbeek, M.,

Lobascio, C., Nebiolo, M.: Post-flight analysis of materials exposed on the spectrometer sub-unit of MEDET (18 months on-board ISS). In: Kleiman, J.I., Tagawa, M., Kimoto, Y. (eds.) Protection of materials and structures from the space environment, p. 41. Springer, Heidelberg (2013)

18. Picone, J.M., Hedin, A.E., Drob, D.P., Aikin, A.C.: NRLM-SISE-00 empirical model of the atmosphere: Statistical comparisons and scientific issues. J. Geophys. Research **107**(A12), SIA15-1-5SIA15-16 (2002)

19. deGroh, K.K., Private communication. Also Pippin, G., Technical operations support (TOPS) II delivery order 0011: Summary status of MISSE-1 and MISSE-2 experiments and details of estimated environmental exposures for MISSE-1 and MISSE-2," AFRL-ML-WP-TR-2006–4237, July 2006

20. Imamura, S., Utashima, M., Ozawa, T., Akiyama, K., Sasaki, M.: Current status of the on-going orbit transfer of super low altitude test satellite (SLATS). In: Proceedings of the 69th International Astronautical Congress, IAC-18-C1.8.1. Bremen, Germany, 2018

21. Tsuchiya, Y., Yukumatsu, K., Goto, A., Miyazaki, E., Kimoto, Y., Imamura, S., Miura, T., Sasaki, M., Operation results of atomic oxygen fluence sensor (AOFS) aboard SLATS satellite.

In: Proceedings of 64th Symposium on Space Science and Technology, JSASS-2020–4266 (2020) in Japanese

22. Sauerbrey, G.: Verwendung von schwingquarzen zur wägung dünner schichten und zur mikrowägung. Z. Phys. **159**, 206–222 (1959)

23. Miyoshi, Y., Fujiwara, H.: A study on neutral density in the thermosphere using SLATS and a numerical model. In: Proceedings of 64th Symposium on Space Science and Technology, JSASS-2020–4450 (2020) in Japanese

24. Bowman, B.R., Tobiska, W.K., Marcos, F.A., Huang, C.Y., Lin, C.S., Burke, W.J.: A new empirical thermosphreic density model JB2008 using new solar and geomagnetic indices, In AIAA/AAS astrodynamics specialist conference and exhibit, 2008

25. Bruinsma, S.L.: The DTM-2013 thermosphere model. J. Space Weather Space Clim. **5**, A1 (2015)